International Journal of Pharmaceutics 468 (2014) 264–271

Contents lists available at ScienceDirect

International Journal of Pharmaceutics

journal homepage: www.elsevier.com/locate/ijpharm

Pharmaceutical Nanotechnology

# Construction and physiochemical characterisation of a multi-composite, potential oral vaccine delivery system (VDS)

Marie W. Pettit [a], Paul D.R. Dyer [a], John C. Mitchell [d], Peter C. Griffiths [a], Bruce Alexander [a], Beatrice Cattoz [a], Richard K. Heenan [b], Stephen M. King [b], Ralf Schweins [c], Frank Pullen [a], Stephen R. Wicks [d], Simon C.W. Richardson [a,*]

[a] Faculty of Engineering and Science, University of Greenwich, Central Avenue, Chatham Maritime, Kent ME4 4TB, UK
[b] ISIS Facility, STFC Rutherford Appleton Laboratory, Harwell Oxford, Didcot OX11 0QX, UK
[c] Institut Laue - Langevin, DS/LSS, CS 20 156, Grenoble CEDEX 9 F-38042, France
[d] Medway Centre for Pharmaceutical Sciences, Faculty of Engineering and Science, University of Greenwich, Central Avenue, Chatham Maritime, Kent, ME4 4TB, UK

ARTICLE INFO

*Article history:*
Received 6 February 2014
Received in revised form 19 March 2014
Accepted 25 March 2014
Available online 26 March 2014

*Keywords:*
Vaccine
Enteric
Immobilisation
Silica
Synthetic protein

ABSTRACT

An increasing human population requires a secure food supply and a cost effective, oral vaccine delivery system for livestock would help facilitate this end. Recombinant antigen adsorbed onto silica beads and coated with myristic acid, was released (~15% (w/v)) over 24 h at pH 8.8. At pH 2, the myristic acid acted as an enteric coating, protecting the antigen from a variety of proteases. The antigen adsorbed onto silica particles, coated in myristic acid had a conserved secondary structure (measured by circular dichroism (CD) spectroscopy) following its pH-triggered release. Small angle neutron scattering (SANS) was used to measure the thickness of the adsorbed antigen, finding that its adsorbed conformation was slightly greater than its solution radius of gyration, *i.e.* 120–160 Å. The addition of myristic acid led to a further increase in particle size, with scattering data consistent with an acid thickness slightly greater than a monolayer of fully extended alkyl chains and a degree of hydration of around 50%. Whilst adsorbed onto the silica and coated in myristic acid, the protein was stable over 14 days at 42 °C, indicating a reduced need for cold chain storage. These data indicate that further investigation is warranted into the development of this technology.



## 1. Introduction

The human population is predicted to reach 10 billion by 2050 (Cohen, 2003) and needs to be able to not only feed itself, requiring the ablation of disease in livestock, but also combat infectious disease in densely populated areas. Consequently, there exists enormous humanitarian value in developing effective oral vaccine delivery systems for both the clinical and veterinary arenas. Barriers to successful oral vaccination include; (i) the proteolytic environment of the gastrointestinal (GI) tract (*i.e.* the stomach or its equivalent in livestock, as well as commensal bacteria inhabiting the large and small intestine) and (ii) inefficient antigen presentation which may involve either translocation into the underlying *lamina propria* (LP) (containing dendritic, antigen presenting cells (APCs)) (Clayton et al., 2006) or uptake by the Peyer's patch (PP), evading mucus lining the lumen. In an attempt to circumvent these obstacles, large doses of antigen have been administered orally (Kunisawa et al., 2012) and this approach has met with limited success. Equivalently, live attenuated viral vaccines have been used and despite some success, concerns have been raised regarding safety due to either viral reversion to virulence or viral propagation. Additionally, viral vaccines are expensive to produce as well as being difficult to store and administer (Shaw and Davidson, 2000) and may also reduce the yield from livestock (Müller et al., 2012).

Unstable "soft" systems fabricated from poly(lactide-co-glycolide), chitosan or alginate micro- or nano-particles may extend antigen gut residence time, reduce gastric and intestinal

*Abbreviations:* SANS, small angle neutron scattering; CD, circular dichroism; APCs, antigen presenting cells; LP, lamina propria; PP, Peyer's patch; VDS, vaccine delivery systems; GST–GFP, glutathione-S-transferase (GST) fused in frame with green fluorescent protein (GFP); MALDI-TOF, matrix assisted laser desorption ionisation time of flight; BCA, bicinchoninic acid assay; IPTG, isopropyl β-D-1-thiogalactopyranoside; SDS PAGE, sodium dodecyl sulphate polyacrylamide gel electrophoresis; MDA, maternally derived antibodies.

* Corresponding author: Tel.: +44 208 331 8207; fax: +44 208 331 9805.
*E-mail address:* S.C.W.Richardson@Greenwich.ac.uk (S.C. Richardson).

http://dx.doi.org/10.1016/j.ijpharm.2014.03.046
0378-5173/

degradation, whilst enhancing absorption and reducing the amount of antigen required to elicit an immune response. These systems typically have either entrapped or surface adsorbed antigen (Wilkhu et al., 2011; Mercier et al., 2007). However, premature release or hydrolysis of the antigen *in situ* has led to antigen degradation prior to presentation to the immune system *i.e.* uptake by APCs or by the PPs. Non-degradable nanoparticulate gold or silica has been used to immobilise antigens intended for oral vaccination (Wang et al., 2012; Tang et al., 2011). Nano-particulate silica has been proposed as a component of medicines designed to treat diseases affecting bone, tendons, diabetes, inflammation and cancer (Vallet-Regi and Ruiz-Hernandez, 2011). Since, in this instance, nano-particulate silica would be delivered orally, it was hypothesised that the vaccine delivery systems (VDS) proposed herein would not be subject to trans-cytosis across the epithelial lining of the gut. This is due to its diameter being too big for the clathrin or caveolae-mediated cellular uptake (dos Santos et al., 2011) necessary for transcytosis (Tuma and Hubbard, 2003) (*i.e.* greater than 2–300 nm). Silica has also been shown to exhibit low toxicity at concentrations of up to 500 μg/ml in macrophages (Herd et al., 2013) and is amenable to surface functionalisation, making it an attractive delivery system component (Wen et al., 2013).

In an effort to stabilise adsorbed proteins through the proteolytic environment of the GI, the encapsulation of silica adsorbed antigen has been attempted using polymers such as poly (acrylic acid). The polymer coat designed to be unstable at higher pH (*i.e.* within the lumen of the small intestine) whilst being stable at low pH (*i.e.* within the stomach) (Song et al., 2007) provided a smart, enteric, antigen controlled release system. The aforementioned systems often have demonstrated low bioavailability profiles (Sakuma et al., 1997) and consequently, myristic acid, previously used as a food additive, extracted from nutmeg (Burdock and Carabin, 2007) was evaluated as an enteric coat.

The system was characterised by determining the size of the silica as well as the antigen (a recombinant protein) corona. The size of the myristic acid coated antigen adsorbed silica was also determined. The effectiveness of the myristic acid coat to protect the underlying protein antigen from protease K and an *in vitro* stomach model was also assessed. Protein release was documented as a function of pH and the secondary conformation of the protein antigen (glutathione-S-transferase fused in frame with green fluorescent protein (GST–GFP)), was monitored in the native form as well as post-release (with and without myristic acid coating). The conservation of protein conformation may, in this instance, be used to drive both transcytosis and antigen uptake, mediating immunisation. Finally, antigen stability was also assessed over a defined time period (14 days) above ambient temperature (42 °C) in order to assess the impact of formulation upon vaccine cold-chain storage.

## 2. Materials and methods

### 2.1. Materials

#### 2.1.1. Equipment

The orbital shaker and microtitre plate reader were from Thermo Fischer, (Loughbourgh, UK). The mini-PROTEAN® tetra cell, mini *trans*-blot, electrophoretic transfer cell and PowerPac HC™ power supply were supplied by BioRad (Hemel Hempstead, UK). The French Press and Sorvall® RC6 Plus, centrifuges were from ThermoFisher Scientific (Loughborough, UK). The matrix assisted laser desorption ionisation time of flight (MALDI-TOF) mass spectroscopy was performed on an Autoflex MALDI-TOF system (Bruker, Coventry, UK). The freeze dryer (Wizard 2.0 VirTis) was supplied by SP Scientific (Suffolk, UK). The Chirascan™ was supplied by Applied PhotoPhysics, (Surrey, UK). The zeta seizer (Nano Z) was supplied by Malvern (Worcestershire, UK). Small angle neutron scattering was performed in 2 mm path length cylindrical ("banjo") fused silica cuvettes (Hellma GmbH & Co., Müllheim, Germany). Fluorescence spectra were measured using a Fluoromax-4 spectrofluorometer (Horiba Scientific, Middlesex, UK).

#### 2.1.2. Reagents

General Laboratory reagents were purchased from Sigma (Dorset, UK). Specialised reagents: bicinchoninic acid assay (BCA) assay kit, glucose, ampicillin, reduced glutathione, isopropanol, tris-base, PBS tablets, lithium chloride, ethylenediaminetetraacetic acid di-sodium salt (EDTA), glycerol, agarose, sodium hydroxide, potassium acetate, ammonium acetate, pancretin, porcine bile, myristic acid, guanidinium HCl, acetone, pepsin, isopropyl β-D-1-thiogalactopyranoside (IPTG), protease K, sodium azide, nitrocellulose membrane (0.2 μm pore size) and bovine serum albumin (BSA) were purchased from Sigma (Dorset, UK). Coomassie brilliant blue G-250, acrylamide, bis-acrylamide, ammonium persulphate, 2-mercaptoethanol, sodium dodecyl sulphate (SDS) were purchased from BioRad (Hemel Hempstead, UK). Tris-base, Bacto-tryptone, Bacto-yeast extract, ampicillin, glycerol, imidazole, sodium chloride, and glycine were purchased from Fischer (Leicestershire, UK). $Ni^{2+}$ Sepharose™ (high-performance) was supplied by GE Healthcare (Buckinghamshire, UK). Silicon(IV) oxide powder, (0.5 micron), was supplied by Alfa Aesar (Lancashire, UK).

### 2.2. Recombinant protein production

The plasmid (pGST–GFP (GenBank JN232535.1)) has been described in detail previously (Urbanowski and Piper, 1999) and was a kind gift from Professor Robert Piper (University of Iowa, USA). For protein expression, pGST–GFP was transformed into *E. coli* MC1061 (Invitrogen, Paisley, UK) and grown overnight (to saturation) in 2xYT media containing 25 μg/ml ampicillin with or without deuterium oxide in place of water. The latter was used to produce partially deuterated protein. The saturated 10 ml overnight culture was used to inoculate 1000 ml of 2xYT media containing 25 μg/ml ampicillin, which was grown at 37 °C shaking at 180 rpm for 4 h. Gene expression was induced by adding IPTG (1 μM), and continuing to incubate the culture for a further 4 h at 37 °C shaking at 180 rpm. The bacteria were lysed using a French Press pressure cell (ThermoFisher Scientific, Loughborough, UK) set to 1500 psi, cleared by sedimentation at 20,000 × *g* (4 °C) and subject to affinity enrichment using glutathione-conjugated Sepharose 4b (GE Healthcare, Bucks, UK), in accordance with the manufacturer's instructions. Sodium azide (0.2% (w/v)) and a 5× concentration of protease inhibitors (Complete™ EDTA free protease inhibitor cocktail (Roche, Burgess Hill, UK)), were added after the lysis of the *E. coli* MC1061. Enriched protein was then dialysed against PBS.

### 2.3. Recombinant protein characterisation

After GST–GFP enrichment (Section 2.2), protein concentration was determined using the BCA assay against BSA standards. Care was taken to ensure the readings were within the linear range of the assay. Having assessed protein concentration, GST–GFP fluorescent spectra was recorded by first determining the protein's absorption profile. Having determined the wavelength at which maximum absorption (lambda maximum) occurred (490 nm), this wavelength was then used to excite the protein sample to determine the emission profile.

#### 2.3.1. SDS PAGE and Coomassie R-250® brilliant blue staining

Affinity enriched GST–GFP (Section 2.2) was further characterised by sodium dodecyl sulphate polyacrylamide gel electrophoresis (SDS PAGE) and Coomassie G250® brilliant blue staining

in order to determine (i) the degree of protein enrichment and (ii) the apparent molecular weight of the protein (Fig. 1 (panel a). This was performed in accordance with the mini-protein Tetra Cell manufacturers instructions (BioRad, Hemel Hempstead, UK).

*2.3.2. Western blotting and imumunodetection*

Immobilised protein was obtained by separating protein samples using SDS PAGE (Section 2.3.1) and electroblotting using the mini *trans*-blot, electrophoretic transfer cell (BioRad, Hemel Hempstead, UK) and following the manufacturer's instructions. Protein detection was performed using both GFP- (A11122, Invitrogen, Paisley, UK) and GST-specific (ab19256, Abcam, Cambridge, UK) monoclonal, primary antibodies (Fig. 1 (panel a)). Antibody detection was performed using a horseradish peroxidase-conjugated secondary antibody (mouse IgG specific) and picostable enhanced chemiluminescence reagent (GE Healthcare, Bucks, UK) in accordance with the manufacturer's instructions.

*2.3.3. MALDI-TOF mass spectroscopy*

MALDI-TOF MS was performed using an Autoflex MALDI-TOF system (Bruker, Coventry, UK). Protein identification by peptide mass fingerprinting was also carried out to obtain GST–GFP sequence information. To this end, GST–GFP was digested with trypsin following standard procedures (Cottrell, 1994). The resulting digest mixture was analysed by MALDI-TOF MS and the experimental mass values were compared with reference peptide mass values, calculated by applying the enzyme cleavage rules (Pappin et al., 1993).

*2.4. Protein immobilisation*

Purified, recombinant protein (GST–GFP) (10 mg) was incubated with silica beads (Alfa Aeser, Lancashire, UK) (1 mg) in sodium acetate buffer (pH 5.6) on a rotating rack at 4 °C overnight. The protein-adsorbed silica was subject to sedimentation at 6000 × *g* for 2 min. Supernatant was removed and two washes with sodium acetate buffer were performed to remove any non-bound protein. Non-bound protein was analysed using the BCA assay and adsorption plots derived.

*2.5. Myristic acid coating*

Serial dilutions of myristic acid were performed to explore the effects of surface coverage, spanning sub-monolayer through to the multi-layer deposition of myristic acid. Protein adsorbed silica beads (Section 2.4) were immersed in 5 ml pentane containing the indicated amounts myristic acid. Pentane was allowed to evaporate during sonication at 23.5 W/cm$^2$ for 30 min or until the pentane had evaporated. Myristic acid coated particles were then freeze-dried using a VirTis Wizard 2.0 freeze dryer (thermal cycles as described (see Supplementary data)). Unless otherwise noted (*i.e.* during the SANS experiments) 1 mM myristic acid/g silica was used to coat the antigen adsorbed silica (Section 2.4).

*2.6. Particulate characterisation*

*2.6.1. Assessment of particle composition using zeta sizing*

Measurements were taken using a 1 ml volume and ten repeats were performed to maximise the signal to noise ratio. The

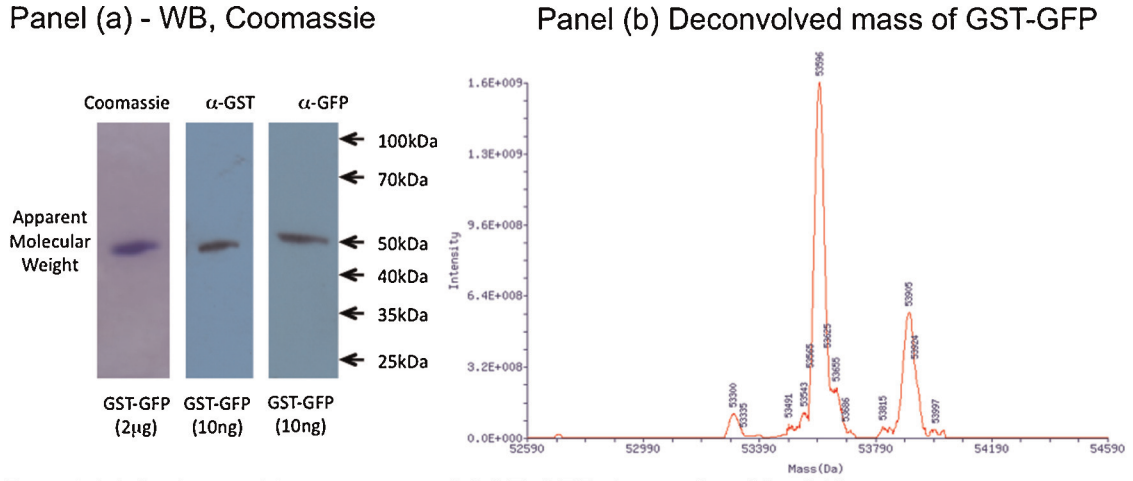


Panel (c) Amino acid sequence of GST-GFP determined by MS

MSPILGYWKIKGLVQPTRLLLEYLEEKYEEHLYERDEGDKWRNKKFELGLEFPNLPYYIDGDVKLTQSMAIIR
YIADKHNMLGGCPKERAEISMLEGAVLDIRYGVSRIAYSKDFETLKVDFLSKLPEMLKMFEDRLCHKTYLNG
DHVTHPDFMLYDALDVVLYMDPMCLDAFPKLVCFKKRIEAIPQIDKYLKSSKYIAWPLQGWQATFGGGD
HPPKSDLIEGRGIPGNSSMASKGEELFTGVVPILVELDGDVNGHKFSVSGEGEGDATYGKLTLKFICTTGKLP
VPWPTLVTTFSYGVQCFSRYPDHMKRHDFFKSAMPEGYVQERTISFKDDGNYKTRAEVKFEGDTLVNRIE
LKGIDFKEDGNILGHKLEYNYNSHNVYITADKQKNGIKANFKIRHNIEDGSVQLADHYQQNTPIGDGPVLLP
DNHYLSTQSALSKDPNEKRDHMVLLEFVTAAGITHGMDELYKSGSGPVLAVPSSDPLVQCGGIALKGNSA
DIQHS GGRSSLEGPFKPADQPRLCLLVASHLLFAPPPCLP.

**Fig. 1.** Fig. 1 documents the characterisation of the recombinant antigen used herein (GST–GFP). Enriched GST–GFP was analysed by SDS PAGE and Coomassie staining, Western immunoblotting using primary antibodies specific for both GST and GFP (panel a) and MALDI-TOF MS (panel b) as well as via the analysis (by MS) of tryptic fragments from GST–GFP, mapped back to the predicted sequence (derived from the plasmid GenBank JN232535.1) (panel c). The entire predicted protein sequence derived from the GST–GFP ORF within pGST–GFP (JN232535.1) is shown. The amino acids in red were identified as tryptic fragments within GST and the area in blue, within GFP. The area in black was not identified as being covered by tryptic fragments. (For interpretation of the references to colour in this figure legend, the reader is referred to the web version of this article.)

temperature was set to 21 °C and allowed to equilibrate for thirty minutes before the samples were loaded.

*2.6.2. Assessment of particle composition using small angle neutron scattering (SANS)*

SANS experiments to assess the diameter of the silica and silica-adsorbed protein (Section 2.4) were performed on instrument D11 (lowest momentum transfer and lowest background instrument) at the Institut Laue – Langevin, Grenoble, France. The scattering was measured in 2 mm Hellma cells placed within a rotating rack, to obviate the slow settling that occurs within these systems. Three sample detector distances (1.2, 8 and 39 m), with appropriate collimation, were employed, using incident neutrons with wavelength 8 Å. Data were normalised by reference to a flat scatterer (1 mm $H_2O$ at ILL, flood source at ISIS) and then adjusted to absolute scattering cross sections by reference to a standard sample.

The data describing the myristic acid coated, antigen adsorbed silica (Section 2.5) was collected using the SANS 2D beamline at the ISIS pulsed neutron source, Didcot, UK, also using 2 mm Hellma cells placed in a rotating rack. The SANS data from both instruments were ultimately fitted to an analytical multi-shell model, assuming a spherical geometry using the program FISH (Heenan, 1989).

*2.7. Protein stability assay*

*2.7.1. Protein stability assay using protease K*

Initially the sensitivity of GST–GFP to protease K was established. As the fluorescence of the GFP portion of the GST–GFP protein was found to persist after protease digestion (500 μg GST–GFP with 100 μU of protease K in PBS incubated for 60 min at 37 °C shaking at 180 rpm) (Section 2.2), a GST "pull down" (sedimentation) assay was used to assess protein integrity followed by Western immunoblotting (to monitor molecular weight). This assay was performed using glutathione-conjugated Sepharose 4b to sediment (21,000 × *g* for 60 s at room temperature) intact protein from the digestion reaction (the supernatant was discarded) prior to Western immunoblotting performed as previously described. This experiment allowed an assessment of the unit value of protease appropriate for the digestion of a known amount of GST–GFP immobilised upon the silica, as well as providing a positive control for protease K mediated digestion. To assay immobilised and myristic acid coated antigen stability, 100 μU of protease K was incubated with 500 μg equivalent of protein-adsorbed silica in PBS at 37 °C for 60 min (Fig. 3). Where indicated the samples were kept in a humidified atmosphere at 42 °C for 14 days prior to digestion and analysis by Western immunoblotting using a GFP-specific primary antibody (Section 2.3.2).

*2.7.2. Protein stability assay using an in vitro stomach model*

Myristic acid coated, protein adsorbed silica (Section 2.5) was placed in HCl (0.1 M) with pepsin (40 μg/ml) (Sigma, Dorset, UK) (Glahn et al., 1998). After an hour, $NaHCO_3$ (0.1 M) was used to neutralize the pH (pH 7.4) and porcine bile (12 μg/ml) (Sigma, Dorset, UK) and pancreatin (2 μg/ml) (Sigma, Dorset, UK) was added, simulating lumen of the duodenum. After incubation in the *in vitro* simulated stomach model (4 h, 37 °C), results were analysed by Western immunoblotting and densitometry (Section 2.2 and 2.3.2).

*2.8. Protein release assay*

Freeze dried, myristic acid coated, protein absorbed silica (Section 2.5), was incubated in PBS over the indicated pH ranges, at 37 °C for 2 h (Fig. 4 (panel a)). After this time the sample was sedimented at 6000 × *g* for 2 min at room temperature. The supernatant was then collected and analysed for release studies, via Western immunoblotting and BCA assay. Protein that remained adsorbed to silica beads was analysed via Western immunoblotting, and mass balance performed, again by Western immunoblotting. Protein was quantified by densitometry using ImageJ (NIH, Maryland, USA).

*2.9. Analysis of protein structure by circular dichroism spectroscopy*

Released protein was inserted into a 0.1 mm quartz cuvette (approximate concentration of 0.2 mg/ml) and analysed at wavelengths between 190–260 nm, bandwidth 1 nm, 20 °C in PBS. Blank (PBS) was subtracted from the data and plots obtained using Prism software (GraphPad, California, USA).

## 3. Results

*3.1. Protein characterisation*

Having isolated highly enriched (*i.e.* one protein band visible in an SDS PAGE Coomassie stained gel), recombinant, GST–GFP from *E. coli* MC1061 lysate, the protein antigen, was characterised by Western blotting and immunodetection (Fig. 1 (panel a)) and also mass spectroscopy (Fig. 1 (panel b and c)). The protein was immunoreactive to both GST- and GFP-specific antibodies and in a departure from the mass predicted from an *in silico* analysis of the plasmids sequence, the mass and amino acid sequence of the protein was determined following a tryptic digest (Fig. 1 (panel c)). The deconvolved MALDI-TOF data described the enriched GST–GFP protein to have a mass of 53.6 kDa (Fig. 1 (panel c)), corroborating the data from the gel electrophoresis experiments including Western analysis. The variance from the *in silico* data (from GenBank JN232535) is very likely due to GST–GFP missing the N-terminal methionine and the 69 C-terminal amino acids, which would give a mass of 53,600.00 Da *versus* the observed mass of 53600.22 Da. Given that the missing portion of the protein was derived from *Plasmodium* spp., rather than from GFP, the omission was deemed of no consequence to this study. The fluorescence emission spectrum of GST–GFP was identical to the published spectra of GFP (Pollok and Heim, 1999) (data not shown).

*3.2. Particle characterisation*

Approximately 75% of GST–GFP (500 μg) was adsorbed onto the silica beads (50 mg) by decreasing the pH to 5.6 in sodium acetate buffer as analysed by BCA assay (Section 2.5). Thus, a 1:10 ratio of protein:silica was required for optimal protein loading. Unique to this work, pentane was used as a solvent for the myristic acid and also used to coat the protein-adsorbed silica. The silica, antigen adsorbed silica and the antigen adsorbed, myristic acid coated silica were characterised using SANS and by assessing zeta potential. SANS defined the silica to be approximately 6600 ± 290 Å in diameter, at the upper most end of the scale quantifiable by SANS, but comparable with the light scattering estimate (silica diameter 6230 Å). However, SANS was used to characterise the thickness of the protein corona surrounding the silica using a series of contrast-matched samples (Fig. 2), requiring both deuterated and hydrogenated GST–GFP. Contrast variation allowed the relative scattering from the core particle and protein coat to be independently varied. The multiple datasets were then simultaneously fitted to a single parameterised model to greatly increase the delineation of the quantities returned in the fitting. Taken together, the SANS data has shown that the protein coated silica particles appeared discrete, (*i.e.* not aggregating), with a corona of adsorbed protein measuring 120–160 Å (12–16 nm). The

absolute intensities are entirely consistent with these dimensions and the known composition of the system, suggesting a water content within the protein layer of some 30–40% (w/v). The thickness of the protein layer is approximately double the theoretical GST–GFP radius of gyration (8.4 nm) (calculated using I-TASSER (Roy et al., 2010)) consistent with polymer adsorption theories (Fleer et al., 1993). These values are also in good agreement with the zeta sizing data, describing the protein-adsorbed silica's diameter to be approximately 6310 Å, showing an increase in particle size of $10 \pm 3.2$ nm upon protein adsorption.

The above system was similarly characterised by SANS after protein adsorption and myristic acid coating with 473 μM of myristic acid/g silica (affording almost 100% protease protection (Fig. 3)). As before, the samples had to be continually rotated whilst suspended in solution on the beamline. The data presented in Fig. 2 (panels c and d), were analysed taking the particle/protein layer analysis as a starting point (King et al., 2000). Two contrasts against deuterium oxide were examined, one in which the protein was hydrogenous and there were no distinct steps in the scattering length density profile ($\rho_{particle} = 3.6 \times 10^{-4}\,nm^{-2}$, $\rho_{protein}$ = (partially deuterated) $4.0 \times 10^{-4}\,nm^{-2}$, (hydrogenated) $2.0 \times 10^{-4}\,nm^{-2}$, $\rho_{acid} = 3.2 \times 10^{-4}\,nm^{-2}$), the second where the protein was deuterated introducing a step at both the silica/protein and protein/myristic acid interfaces. Taken together, best fits were observed when the thickness of the hydrated protein layer was held at 120 Å ($(\varphi)$ $H_2O$ 50%) with the thickness of the enteric layer around 20 Å, comparable to the fully extended length of the molecule. The absolute scattering intensities, whilst imprecise due to the sample instability, suggest that the enteric coating is also hydrated to a level of around 50%.

### 3.3. Enteric protection, protein release and analysis

To characterise the degree of protection provided by the myristic acid coat, a series of samples were prepared that spanned an input of 10 pM–1 mM myristic acid/g silica (Fig. 3). Optimal protection was observed (*i.e.* ~100% (w/v) protein recovery after incubation with 500 μU of protease K at 37 °C for 1 h) after coating with 1 mM myristic acid/g of protein-adsorbed silica (Fig. 3 (panel a)). Further protection is evident from an *in vitro* digestion model simulating the stomach, after the VDS was sonicated during myristic acid coating (but not after stirring during myristic acid coating) (Fig. 3 (panel a)). At quantities below 1 mM myristic acid, protein degradation was evident (Fig. 3 (panel b)). At a myristic acid concentration above 1 mM, the myristic acid coated, protein adsorbed silica was stable over 2 weeks at 42 °C (Fig. 3 (panel b)).

After myristic acid coating, protein remained adsorbed to the silica surface at pH 3.6 and pH 5 and was released at pH 8.8 (7% (w/v) after 2 h at 37 °C (Fig. 4 (panel a)). Released protein was

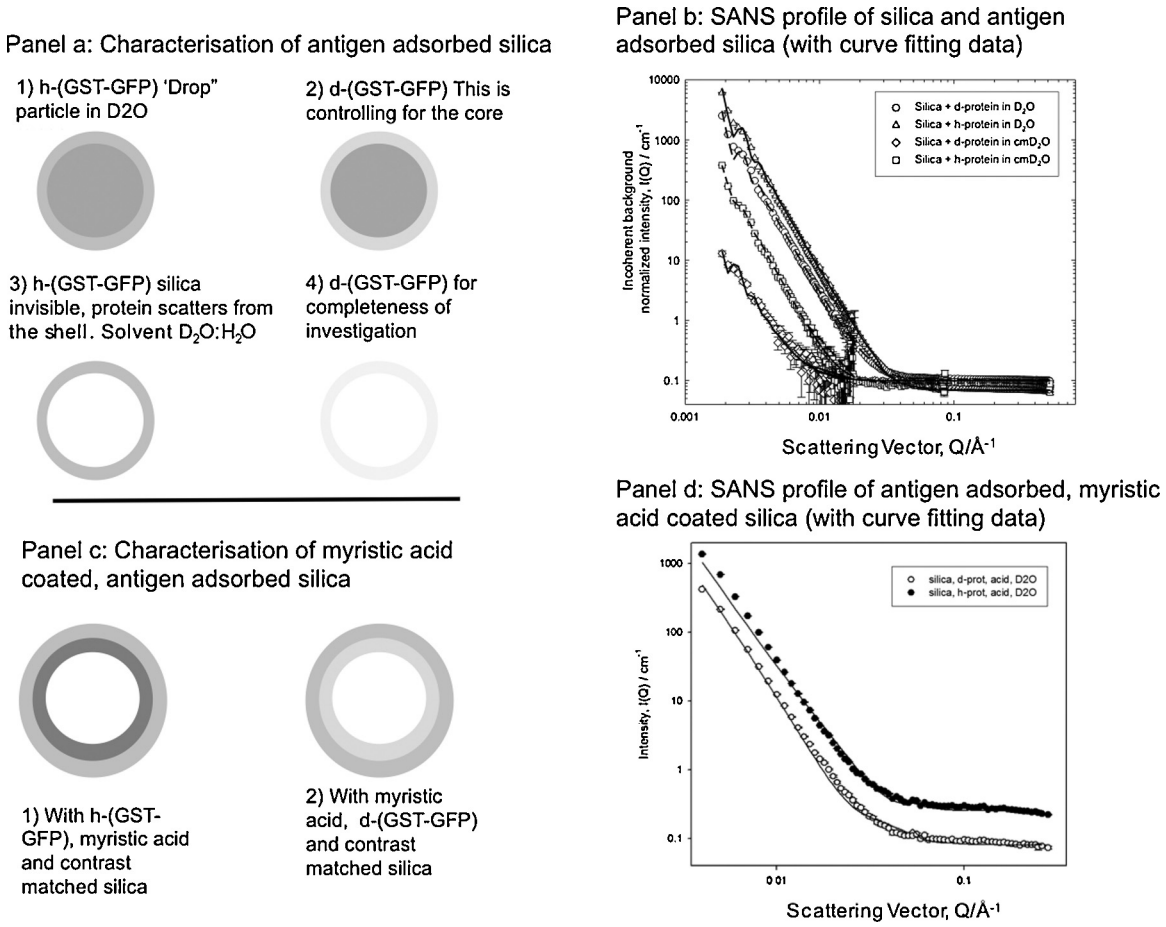


**Fig. 2.** Fig. 2 shows the characterisation of the VDS described herein by SANS. Panel (a) defines a series of contrast matching experiments used to define the protein corona adsorbed onto the silica particles. Panel (b) records the SANS data and "mathematical fits" *i.e.* a core–shell model, (Guinier and Fournet, 1955) describing the experiment previously outlined (in panel a). Panel (c) describes the SANS experiment designed to measure the extent of protein coating, utilising both deuterated and hydrogenated GST–GFP. Panel (d) describes the SANS data and the associated modelling of the "mathematical fit" that best describes the diameter of the VDS after myristic acid coating using 437 μM of myristic acid/g silica. These data describe a particle with mean diameter $6600 \pm 290$ Å and a protein corona of 120–160 Å. The myrisitic acid may be measured as a disordered phase approximately 20 Å deep extending beyond the protein corona.

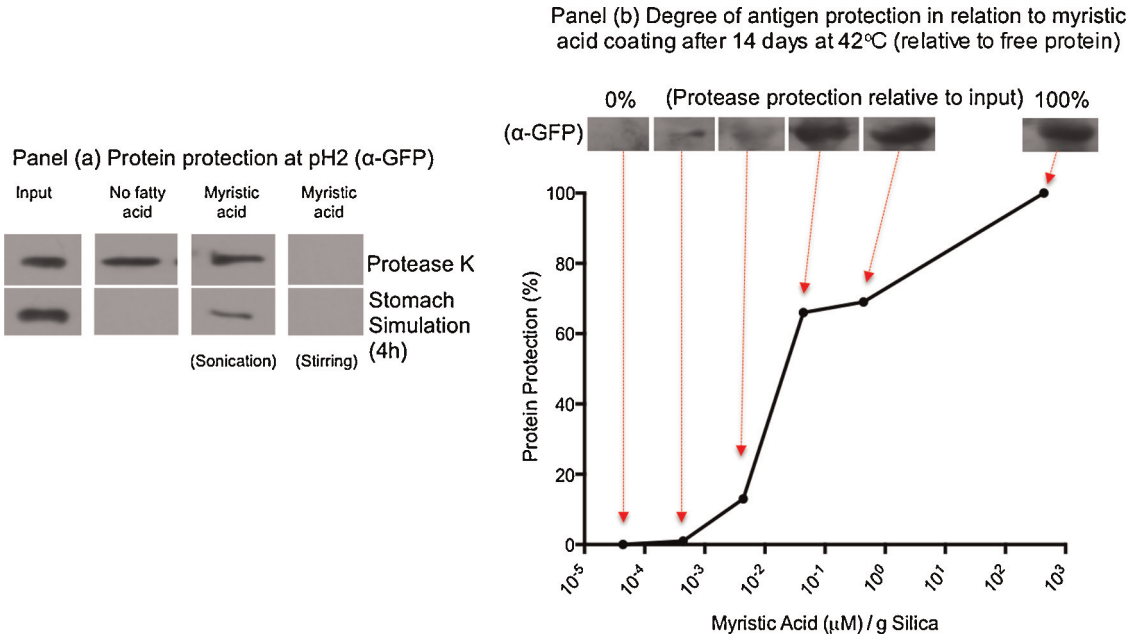


**Fig. 3.** Fig. 3 documents the protection afforded to the protein antigen after varying degrees of myristic acid coating ([Myristic acid]/g silica). Panel (a) documents the protection afforded by the myristic acid coated (1 mM/g silica) to GST–GFP from both protease K (500 μU, digestion over 1 h at 37 °C) and during an *in vitro* stomach simulation (4 h digestion at 37 °C). Panel (b) shows the protection of GST–GFP in relation to a varying amount of myristic acid after 14 days storage at 42 °C. Here 100 μU of protease K was used and the VDS were exposed to the protease K for 1 h at 37 °C. Protein quantitation was performed by Western immunoblotting relative to a set of standards being careful to stay within the linear range of the assay. Representative blots are shown using a GFP specific primary antibody and correspond to the points indicated on the graph (*i.e.* amount of myristic acid used).

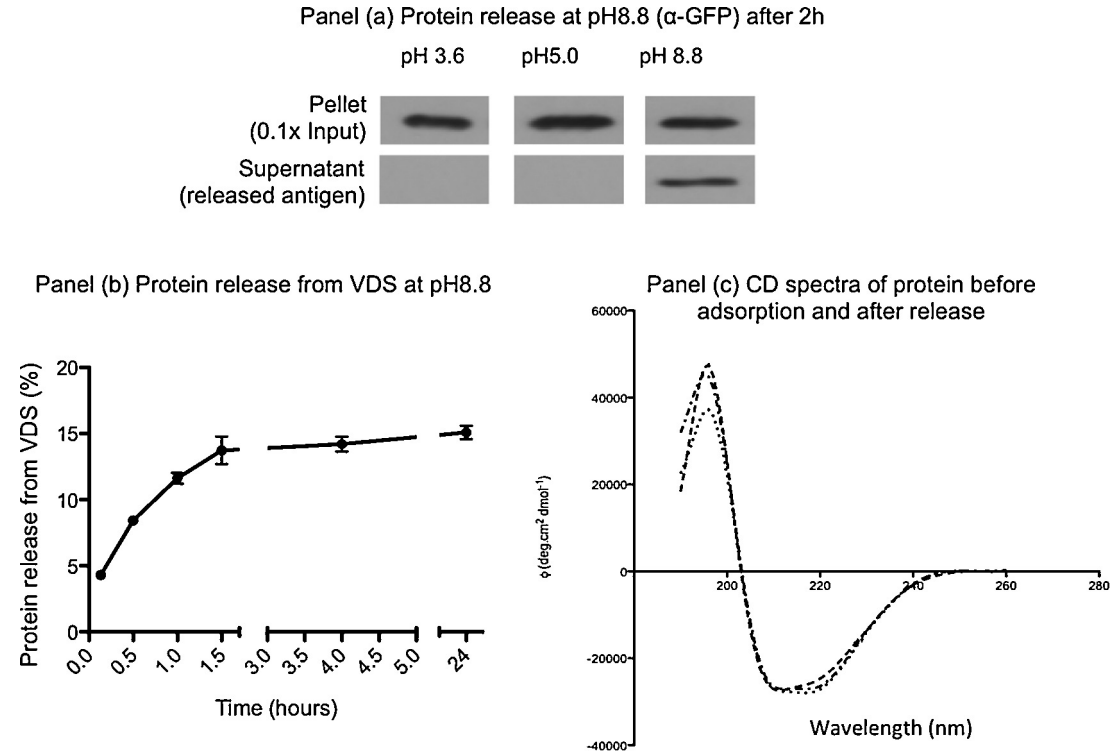


**Fig. 4.** Fig. 4 documents the release of GST–GFP from VDS in response to pH. Panel (a) records release over 24 h. Protein detection was performed by immunoblotting using an anti-GFP polyclonal primary antibody. As was recorded, protein was released from the VDS into the supernatant at pH 8.8 after 2 h. Panel (b) shows protein release from the VDS at pH 8.8 over 24 h. These data show approximately 15% protein release from the myristic acid coated protein (1 mM myristic acid/g silica) adsorbed silica. Fig. 4 (panel c) shows the CD spectra from: protein released from protein-adsorbed myristic acid coated silica (——), the native, unformulated protein (GST–GFP) ( · · · · ) and protein released from protein-adsorbed silica (–·–·–). GST–GFP release from the myristic acid coated silica displayed an almost identical secondary conformation pre- and post-release, with or without myristic acid coating. These data were used to derive molar elipticity for each sample, which was recorded in Table S1.

**Table 1**
CD spectra (molar elipticity) of antigen: pre-adsorption and post-release.

| Molar elipticity | GST-GFP (%) | Released protein | |
|---|---|---|---|
| | | No myristic acid (%) | Myristic acid coat (%) |
| α-Helix | 16.9 | 16.9 | 16.9 |
| β-sheet | 20.8 | 20.8 | 20.8 |
| Random coil | 43.3 | 43.3 | 43.3 |

detected using Western blotting and immunodetection and progressively increased over 90 min before reaching a plateau of up to ~15% (w/v) after 24 h (Fig. 4 (panel b)). The CD spectra of released GST–GFP (Fig. 4 (panel c) and Table 1) demonstrated the conservation of protein secondary structure following its release from the myristic coated VDS.

## 4. Discussion

Fig. 5 depicts a cartoon describing the way this potential VDS may behave based upon the data presented herein. These data have demonstrated the feasibility of using myristic acid coated, antigen adsorbed silica as part of a VDS strategy by characterising both the system in its entirety as well as the protection and release of the protein (antigen) from this system. The technology described herein may provide a way to stabilise protein conformation through the proximal gastrointestinal tract (Fig. 3) and, if applied to a recombinant protein carrier (capable of mediating transcytosis from the lumen of the small intestine (into the LP)), one could envisage a strategy for the oral delivery of vaccine epitopes. Conservation of protein structure is particularly important (Fig. 4), as previous reports have documented antigen conformation being critical for immunisation (Arnold et al., 2003). The conservation of secondary structure post-release (from the VDS), allows the inclusion of recombinant domains that could mediate translocation, from the lumen of the GI into the LP (containing APCs) (Wang et al., 2012). Cholera toxin B chain is reported to provide such "transporter" functionality (Torgersen et al., 2001).

The data describing protein protection in relation to the myristic acid stoichiometry around the so-called Pockels point, is consistent with data from: (i) the SANS experiments (Figs. 2 and 3) and (ii) protection from both protease K and the *in vitro* stomach simulation (Fig. 4). This is assuming a minimum area per fatty acid head group of approximately 20 $Å^2$ (Pockels, 1891) and a spherical surface area of 3.95 $m^2/g$ (after accounting for an additional 12–16 nm protein corona). Given that Pockels point here would be at approximately 33 μM myristic acid/g silica and that the SANS data was performed at a myristic acid input of 437 μM/g silica, the SANS data is consistent with myristic acid coverage slightly in excess of Pockels point. This would point to a fairly inefficient coating methodology. However, as protease protection was evident (Fig. 3), it was deemed adequate. The above data, in conjunction with the predicted degree of hydration of both the protein and fatty acid layer, imply that the lipid coating is not highly ordered. Given the methodology used to coat the particles, this is not entirely unexpected. Furthermore as: (i) protease protection (Fig. 3), (ii) pH-triggered protein release (Fig. 4) and (iii) the release of protein with a highly conserved secondary structure (Fig. 4 and Table 1) was observed, the methodology was again deemed adequate. The specifics governing the interactions between the myristic acid and the protein have not been considered beyond myristic acid deposition in response to the removal of its solvent. This is likely to be very complex interaction, dependant upon protein specific chemistry. Its is an on going subject of investigation and one that will be evaluated once a specific antigen and "transporter" domain have been identified.

It should be noted that the *in vitro* stomach model adopted here does not comply with the standards set by the FDA or in the Pharmacopeia. However, within the context of establishing proof of concept were thought to be adequate.

The experiments described herein (Fig. 3) also described encapsulated, adsorbed protein stability over the experimental time frame (*i.e.* 2 weeks at 42 °C). Although this experiment was not conducted to ICH standards, it provided some preliminary evidence supporting the hypothesis that a consequence of the formulation described may be a reduced need for cold-chain storage (*i.e.* stabilisation), reducing cost.

Myristic acid coating, protease protection and dissolution over the pH range documented were hypothesised to be driven by the $pK_a$ of the myristic acid. Given that the $pK_a$ of myristic acid is 4.9, at pH 2.0 (*i.e.* the pH of the stomach), the myristic acid would be protonated, carrying a net neutral charge. As the pH was neutralised (distal to the stomach), the myristic acid would deprotonate, leaving it with a net negative change driving equilibrium towards dissolution.

The size of the solid phase core material, the release rate of the protein from the solid phase core and the adjuvant effect of the core upon a nominated antigen, will require optimisation in the future. Protein release rate may be further modulated (or optimised) in the future via silica surface functionalisation

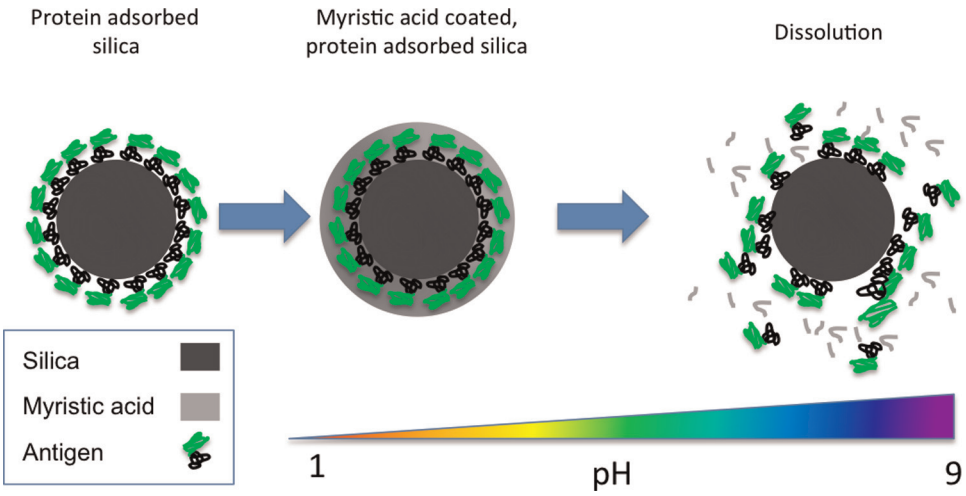


**Fig. 5.** Fig. 5 is a cartoon showing the proposed mode of action of the VDS. A change in pH from the acidic (stomach) to a more alkaline (intestine) environment is proposed to trigger myristic acid and protein dissolution. It was hypothesised that the myristic acid coat could offer protection against proteases.

(Hoffmann et al., 2006) or by manipulating the pI associated with the primary structure of the recombinant protein. However, at this point, it is not known whether the further optimisation of protein release is necessary, as colloids associated with protein antigens may act as adjuvants (Wang et al., 2012). If the VDS size were to be reduced (to less than 100 nm), it may be possible to envisage the entire VDS being transported to the LP (containing APCs), diffusing through the mucus layer (Aljayyoussi et al., 2012), and therefore, eliminating the need for antigen release. Equivalently it may also be possible to use "invasin" family proteins derived from microbes, such as *Yersinia* spp., to augment the uptake of the particle or the released protein into microfold cells of the PP (Tuma and Hubbard, 2003) facilitating antigen presentation to the immune system. Until the efficiencies of the systems described are quantified empirically, it is hard to envisage which will ultimately be the more successful at oral vaccine delivery.

This system may also be amenable to multiple rounds of self administration by large numbers of livestock via mixing it with food, removing the problems associated with the laps in protection from maternally derived antibodies (MDA) seen in species such as *Gallus* spp. as young birds mature (Clench, 1999). As there is little synchronicity associated with the relaxation of MDA associated protection in a flock, multiple rounds of VDS administration might be a cost effective way of overcoming the MDA mediated neutralisation of vaccination. This could be achieved not via the addition of the VDS to drinking water, but by adding the VDS to chicken feed negating the need for specialised supervision over multiple rounds of VDS administration to multiple individuals.

## Acknowledgements

MWP would like to thank the University of Greenwich for her PhD scholarship. SCWR and FP would like to thank Dr Klaus Rumpel and Carla Fernandes for their help with the mass spectroscopy. SCWR and MWP would like to thank Professor Robert Piper (University of Iowa) for the kind gift of the plasmid pGST–GFP. SCR would like to acknowledge grant RB1320038 from the Science and Technology Facilities Council (STFC) which helped support this work.

## Appendix A. Supplementary data

Supplementary data associated with this article can be found, in the online version, at http://dx.doi.org/10.1016/j.ijpharm.2014.03.046.

## References

Aljayyoussi, G., Abdulkareem, M., Griffiths, P., Gumbleton, M., 2012. Pharmaceutical nanoparticles and the mucin biopolymer barrier. BioImpacts 2, 173–174.
Arnold, M., Durairaj, V., Mundt, E., Schulze, K., Breunig, K.D., Sven-Erik, B., 2003. Protective vaccination against infectious bursal disease virus with whole recombinant kluyveromyces lactis yeast expressing the viral VP2 subunit. PLOS 21, 4736.
Burdock, G.A., Carabin, I.G., 2007. Safety assessment of myristic acid as a food ingredient. Food and Chemical Toxicology 45, 517–529.
Clayton, A., Lindon, J.C., Cloarec, O., Antti, H., Charvel, C., Hanton, G., Provost, J.P., Net, J.L., Baker, D., Walley, R.J., Everett, J.R., Nicholson, J.K., 2006. Pharmo-metabonomic phenotyping and personalized drug treatment. Nature Letters 440, 1073–1077.
Clench, M.H., 1999. The avian cecum: update and motility review. Journal of Experimental Zoology 283, 441–447.
Cohen, J.E., 2003. Human population: the next half century. Science 302, 1172–1175.
Cottrell, J.S., 1994. Protein identification by peptide mass fingerprinting. Peptide Research 7, 115–124.
dos Santos, T., Varela, J., Lynch, I., Salvati, A., Dawson, K.A., 2011. Quantitative assessment of the comparative nanoparticle-uptake efficiency of a range of cell lines. Small 7, 3341–3349.
Fleer, G., Cohen Stuart, M.A., Scheutjens, J.M., Crosgrove, T., Vincent, B., 1993. Polymers at Interfaces. Springer ISBN-10: 0412581604.
Ghosh R.E., Egelhaaf S.U., Rennie A.R., 2012. A Computing Guide for Small-Angle Scattering Experiments. Institut Max von Laue. Paul Langevin (ILL06GH05T).
Glahn, R.P., Lee, O.A., Yeung, A., Goldman, M.R., Miller, D.D., 1998. Caco-2 cell ferritin formation predicts nonradiolabeled food iron availability in an *in vitro* digestion Caco-2 cell culture model. Journal of Nutrition 128, 1555–1561.
Guinier, A., Fournet, G., 1955. Small-Angle Scattering of X-Rays. John Wiley and Sons, New York.
Heenan R.K., 1989. FISH Data Analysis Program. RAL Technical Report RAL-89-129.
Herd, H., Daum, N., Jones, A.T., Huwer, H., Ghandehari, H., Lehr, C.M., 2013. Nanoparticle geometry and surface orientation influence mode of cellular uptake. ACS Nano 7, 1961–1973.
Hoffmann, F., Cornelius, M., Morell, J., Froba, M., 2006. Silica-based mesoporous organic-inorganic hybrid materials. Angewangte Chemie International Edition 45, 3216–3251.
King, S.M., Griffiths, P.C., Cosgrove, T., 2000. In: Gabrys, B.J. (Ed.), Applications of Neutron Scattering to Soft Condensed Matter. Gordon & Breach, Amsterdam, pp. 77–105 Chapter 4.
Kunisawa, J., Kurashima, Y., Kiyono, H., 2012. Gut-associated lymphoid tissues for the development of oral vaccines. Advanced Drug Delivery Reviews 64, 523–530.
Mercier, G.T., Nehete, P.N., Passeri, M., Nehete, B.N., Weaver, E.A., Templeton, N.S., Schluns, K., Buchl, S.S., Sastry, J., Barry, M.A., 2007. Oral immuninzation of rhesus macaques with adenoviral HIV vaccines using enteric-coated capsules. Vaccine 25, 8687–8701.
Müller, H., Mundt, E., Eterradossi, N., Islam, M.R., 2012. Current status of vaccines against infectious bursal disease. Avian Pathology 41, 133–139.
Pappin, D.J., Hojrup, P., Bleasby, A.J., 1993. Rapid identification of proteins by peptide-mass fingerprinting. Current Biology 3, 327–332.
Pockels, A., 1891. Surface tension. Nature 43, 437–439.
Pollok, B.A., Heim, R., 1999. Using GFP in FRET-based applications. Trends in Cell Biology 9, 57–60.
Roy, A., Kucukural, A., Zhang, Y., 2010. I-TASSER: a unified platform for automated protein structure and function prediction. Nature Protocols 5, 725–738.
Sakuma, S., Suzuki, N., Kikuchi, H., Hiwatari, K., Arikawa, K., Kishida, A., Akashi, M., 1997. Oral peptide delivery using nanoparticles composed of novel graft copolymers having hydrophobic backbone and hydrophilic branches. International Journal of Pharmaceutics 149, 93–106.
Shaw, I., Davidson, T.F., 2000. Protection from IBDV-induced bursal damage by a recombinant fowlpox vaccine, fpIBDV, is dependent on the titre of challenge virus and chicken genotype. Vaccine 18, 3230–3241.
Song, S.W., Hidajat, K., Kawl, S., 2007. pH-controllable drug release using hydrogel encapsulated mesoporous silica. Chemical Communications 42, 4396–4398.
Tang, H., Guo, J., Sun, Y., Chang, B., Ren, Q., Yang, W., 2011. Facile synthesis of pH sensitive polymer-coated mesoporous silica nanoparticles and their application in drug delivery. International Journal of Pharmaceuticals 421, 388–396.
Torgersen, M.A., Skretting, G., van Deurs, B., Sandvig, K., 2001. Internalization of cholera toxin by different endocytic mechanisms. Journal of Cell Science 114, 3737–3747.
Tuma, P.L., Hubbard, A.L., 2003. Trancytosis: crossing cellular barriers. Physiological Reviews 83, 871–932.
Urbanowski, J., Piper, R.C., 1999. The iron transporter Fth1p forms a complex with the Fet5 iron oxidase and resides on the vacuolar membrane. The Journal of Biological Chemistry 274, 38070–38961.
Vallet-Regi, M., Ruiz-Hernandez, E., 2011. Bioceramics: from bone regeneration to cancer nanomedicine. Advanced Materials 23, 5177–5218.
Wang, T., Jiang, H., Zhao, Q., Wang, S., Zou, M., Cheng, G., 2012. Enhanced mucosal and systemic immune responses obtained by porous silica nanoparticles used as an oral vaccine adjuvant: effect of silica architecture on immunological properties. International Journal of Pharmaceutics 436, 351–358.
Wen, H., Guo, J., Chang, B., Yang, W., 2013. pH-responsive composite microspheres based on magnetic mesoporous silica nanoparticle for drug delivery. European Journal of Pharmaceutics and Biopharmaceutics 84, 91–98.
Wilkhu, J., McNeil, S.E., Kirby, D., Perrie, Y., 2011. Formulation design considerations for oral vaccines. Therapeutic Delivery 2, 1141–1164.